

This article was downloaded by:[Bochkarev, N.]
On: 12 December 2007
Access Details: [subscription number 746126554]
Publisher: Taylor & Francis
Informa Ltd Registered in England and Wales Registered Number: 1072954
Registered office: Mortimer House, 37-41 Mortimer Street, London W1T 3JH, UK



Astronomical & Astrophysical Transactions

The Journal of the Eurasian Astronomical Society

Publication details, including instructions for authors and subscription information:
<http://www.informaworld.com/smpp/title~content=t713453505>

Collapse of non-isothermal, non-adiabatic interstellar clouds

E. I. Vorobyov^a; S. P. Tarafdar^b

^a Astrophysics Department, Rostov State University, Rostov-on-Don, Russia

^b Tata Institute of Fundamental Research, Bombay, India

Online Publication Date: 01 January 1999

To cite this Article: Vorobyov, E. I. and Tarafdar, S. P. (1999) 'Collapse of non-isothermal, non-adiabatic interstellar clouds', *Astronomical & Astrophysical Transactions*, 17:5, 407 - 431

To link to this article: DOI: 10.1080/10556799908244088

URL: <http://dx.doi.org/10.1080/10556799908244088>

PLEASE SCROLL DOWN FOR ARTICLE

Full terms and conditions of use: <http://www.informaworld.com/terms-and-conditions-of-access.pdf>

This article maybe used for research, teaching and private study purposes. Any substantial or systematic reproduction, re-distribution, re-selling, loan or sub-licensing, systematic supply or distribution in any form to anyone is expressly forbidden.

The publisher does not give any warranty express or implied or make any representation that the contents will be complete or accurate or up to date. The accuracy of any instructions, formulae and drug doses should be independently verified with primary sources. The publisher shall not be liable for any loss, actions, claims, proceedings, demand or costs or damages whatsoever or howsoever caused arising directly or indirectly in connection with or arising out of the use of this material.

COLLAPSE OF NON-ISOTHERMAL, NON-ADIABATIC INTERSTELLAR CLOUDS

E. I. VOROBYOV¹ and S. P. TARAFDAR²

¹ *Rostov State University, Astrophysics Department, Zorge 5, Rostov-on-Don,
344104, Russia*

² *Tata Institute of Fundamental Research, Homi Bhabha Road, Bombay-400005,
India*

(Received April 29, 1998)

Using the ZEUS-2D code modified for the purposes of cloud collapse calculations, we explore the dynamics of diffuse interstellar clouds of various masses and initial number densities. We show that heating and cooling processes in interstellar clouds may have a significant effect on their dynamical behaviour. Associated with opacity and photoelectric heating, temperature gradients in the interstellar clouds may assist gravity and lower the Jeans mass. We provide some novel results on how the thermal instability and thermal shock waves can help a low-density, gravitationally stable, diffuse interstellar cloud to evolve into a dense protostellar core which then collapses gravitationally to form a star.

KEY WORDS Interstellar clouds, collapse, numerical methods, hydrodynamics

1 INTRODUCTION

With the advent of millimetre and radio observations along with the observations in UV from satellite-based telescopes, our understanding of star formation processes has improved significantly. These observations have motivated various authors (cf. Elmegreen, 1987; Blitz, 1987; Mouschovias, 1987) to study the formation, structure, and dynamics of interstellar clouds, mostly in their diffuse state. On the other hand, extensive numerical studies on how a cold (~ 10 K) and dense ($\sim 10^{-18}$ g cm⁻³) molecular cloud core can collapse gravitationally to form a star or a binary system (Bodenheimer, 1968; Larson, 1969; Boss and Haber, 1982; Boss and Myhill, 1995, and others) have been undertaken.

The gap between these two extreme studies, namely the question of how a diffuse, gravitationally unbound interstellar cloud can evolve into a protostar core, has recently been filled by the study of Tarafdar *et al.* (1985, 1989) and Prasad, Heere, and Tarafdar (1991). These authors have demonstrated that a diffuse cloud with a mass smaller than the Jeans mass can evolve into a cold, dense core due to

the thermal pressure force which assists gravity. Tarafdar *et al.* (1989) have also attempted to determine the mass–initial number density region where a thermally compressed, diffuse cloud can become gravitationally bound and collapse to form a star. However, they found it difficult to extend their study below the number density of 10 cm^{-3} due to time step limitations. Because they did not include an artificial viscosity in their Lagrangian code, the non-physical oscillations in the post-shock region imposed strict limitations on the time step due to the CFL condition, and the calculations could not be advanced in time.

We have, therefore, used an Eulerian code developed on the basis of the ZEUS-2D code of Stone and Norman (1992, hereafter SN) to examine the behaviour of thermally compressed clouds of low densities. In Section 2, we describe the basic equations as well as some modifications made to ZEUS-2D to improve its efficiency. Also, we provide the results of two tests to show the code reliability for the cloud collapse calculations. In Section 3, we explore the dynamical behaviour of interstellar clouds in the whole mass–initial number density field. We give some novel results on how the thermal instability and thermal shock waves can help a low-density, diffuse interstellar cloud to evolve into a dense protostellar core which then collapses gravitationally to form a star.

2 NUMERICAL ALGORITHMS AND TESTS

2.1 Basic Equations

The hydrodynamical evolution of an interstellar cloud is governed by the following set of partial differential equations

$$\frac{D\rho}{Dt} + \rho \nabla \cdot \mathbf{v} = 0, \quad (1)$$

$$\rho \frac{D\mathbf{v}}{Dt} = -\nabla p - \rho \nabla \Phi - \nabla \cdot \mathbf{Q}, \quad (2)$$

$$\rho \frac{D}{Dt} \left(\frac{e}{\rho} \right) = -p \nabla \cdot \mathbf{v} + \Gamma - \Lambda - \mathbf{Q} : \nabla \mathbf{v}. \quad (3)$$

Here, the dependent variables are the mass density ρ , the velocity \mathbf{v} , and the internal energy density e . The D/Dt denotes the Lagrangian derivative,

$$\frac{D}{Dt} \equiv \frac{\partial}{\partial t} + \mathbf{v} \cdot \nabla. \quad (4)$$

Simple cooling (Λ) and heating (Γ) terms in equation (3) are given by

$$\begin{aligned} \Lambda &= 3.33 \times 10^{-27} T^{0.0987} \exp(-87.87/T) n_H^2 \delta_c \\ &+ 1.7 \times 10^{-24} T^{0.5} \exp(-1.1528 \times 10^5) n_H^2 \delta_c, \end{aligned} \quad (5)$$

$$\Gamma = 10^{-26} n_H \exp(-2 \times 10^{-21} N_H) + 1.1 \times 10^{-28} n_H \mu, \quad (6)$$

where $N_H = \int_r^R n_H dr$ is the column density of hydrogen from the surface of the cloud, δ_c is the depletion factor of carbon, and μ is the cosmic ray ionization rate in units of 10^{-17} s^{-1} . The heating rate constitutes two parts – photoelectric heating and cosmic ray heating. No attempt has been made to include the effect of charge of the dust grains (cf. Draine, 1978). The cooling rate used is a simple cooling due to C II and CO as described by Tarafdar *et al.* (1989). The cooling and heating rates are the approximations to the chemistry balance equations and differ from similar approximations of Bochkarev (1992) only by numerical coefficients.

Note that we have added terms that do not appear in Euler's equations. This is to account for viscous stresses and dissipation due to an artificial viscosity Q . These terms are needed for an adequate treatment of discontinuities that may appear in the flow. The common practice is to use von Neumann and Richtmyer (1950) non-linear artificial viscosity. However, for a cloud collapse problem in spherical geometry (which is most relevant in this case), a tensor artificial viscosity must be used (Tscharnuter and Winkler, 1979; SN). Moreover, for some problems with strong shocks, it has been found that linear artificial viscosity is necessary to damp oscillations which can occur in stagnant regions of the flow (Norman and Winkler, 1986).

The fluid equations with cooling and heating terms are closed by an ideal equation of state which gives the gas temperature T as a function of the mass density ρ and pressure p (the interstellar cloud is assumed to consist of atomic hydrogen only),

$$T = \frac{p}{\rho R}, \quad (7)$$

and by the Poisson equation which determines the gravitational potential,

$$\nabla^2 \Phi = 4\pi G \rho. \quad (8)$$

To solve equations (2) and (3), one also needs the relation between the pressure p and internal energy density e , which is $p = (\gamma - 1)e$ for an ideal gas (SN) with the ratio of specific heats $\gamma = 5/3$ for a monatomic gas.

These equations, written in spherical geometry, are solved using the method of finite differences with a time-explicit, operator split (multistep) solution procedure (SN). By allowing for a moving grid, one can follow global features of the flow (such as collapse or expansion) providing better resolution. Though it appears natural to solve explicitly the internal energy density balance equation (3) with Γ and Λ terms by applying the ZEUS-2D technique, the resulting code is unstable due to the much higher dynamical time scale than that of cooling and heating processes. To achieve stability, one has to decrease the time step to prohibitively small values, so that the calculations cannot be advanced in time. Thus, we have a so-called stiff differential equation and it is well known that the only useful technique to solve this type of equation is to apply time-implicit schemes.

Following the common strategy of the split operator method, we update the internal energy density by splitting equation (3) into two parts. The first part,

the change of the internal energy density e due to advection and pressure work, is computed using the ZEUS-2D code, whereas the second part, the change of e due to heating and cooling, is computed using a fully implicit backward Euler scheme combined with Newton–Raphson (NR) iterations. A fully implicit scheme guarantees stability even if the time step greatly exceeds the cooling and heating time scales. To maintain accuracy, the total change in one time step is kept less than 20%. If this condition is not met, or if the system fails to converge in 10 NR iterations, the time step is reduced, and a solution is once again sought.

It may seem that Lagrangian codes are more relevant for collapse computations. However, we find that for some problems (such as shocks) the grid becomes so highly compressed that it hinders further progress due to the CFL condition and Lagrangian codes become useless. We can overcome this difficulty in the Eulerian codes like ZEUS-2D by choosing a specific grid velocity pattern (e.g. choosing the grid velocity vectors equal to the fluid velocity in the regions free from shocks and setting the grid velocity vectors equal to zero wherever shocks occur).

2.2 The Hydrodynamical Test Problems

2.2.1 Pressure-free Collapse of a Sphere

Standard test suites for hydrodynamic algorithms are widely available (see, e.g., SN). Although we have run all the tests given in the above paper, the results of only the two most relevant to our problem are presented.

The first problem, the gravitational collapse of a homogeneous, pressure-free sphere, is a perfect test for one-dimensional radial advection in spherical coordinates. An analytic solution describes the collapse of every mass shell (Hunter, 1962),

$$(r/r_0) = \cos^2 \beta, \quad (\rho/\rho_0) = \cos^{-6} \beta, \quad (9)$$

where β is obtained from

$$\beta + 0.5 \sin 2\beta = t \sqrt{\frac{8\pi}{3} G \rho(0)}. \quad (10)$$

The free-fall time τ_{ff} , defined as the time at which every mass shell reaches the origin ($r = 0$) simultaneously, occurs when $\beta = \pi/2$ and thus

$$\tau_{\text{ff}} = \sqrt{(3\pi)/[32G\rho(0)]}. \quad (11)$$

Following the work of SN we set up a homogeneous sphere of radius $r = 1$ in spherical coordinates with $\rho = G = 1$ initially, thus obtaining $\tau_{\text{ff}} = 0.543$. To obtain the gradient of the gravitational potential, one can integrate the Poisson equation written for the one-dimensional spherically symmetric case,

$$\left. \frac{d\Phi}{dr} \right|_{r=R} = \frac{1}{R^2} \int_0^R 4\pi G \rho r^2 dr. \quad (12)$$

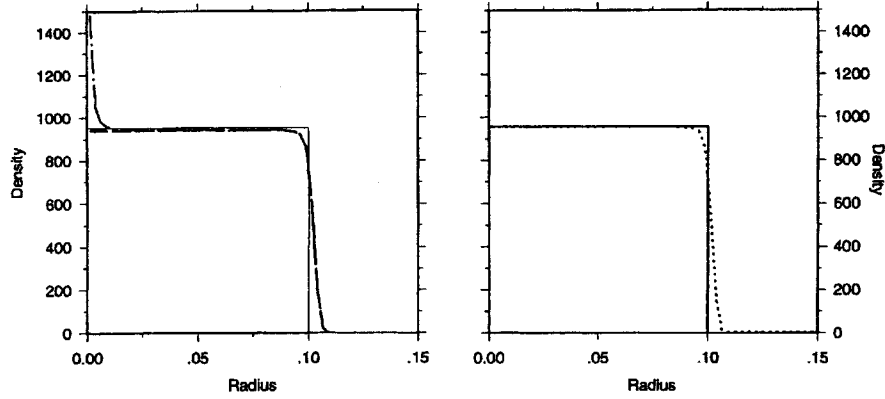


Figure 1 The density distribution for the pressure-free collapse of a homogeneous sphere at $t = 0.985$ free-fall times using a stationary mesh. The dotted-dashed line – the ZEUS-2D code of Stone and Norman (1992); the dashed line – ZEUS-2D with momentum density correction; the dotted line – ZEUS-2D with momentum density and density flux correction. The analytic solution is denoted by the solid line.

Since the density ρ is constant in every grid shell, the above integral can be numerically integrated at every time step,

$$\left. \frac{d\Phi}{dr} \right|_{r=r_i} = \frac{4\pi G}{3r_i^2} \int_{j=1}^i \rho_j (r_{j+1}^3 - r_j^3), \quad (13)$$

where $r_1 = 0$ is the origin.

2.2.2 Momentum Density Correction

The test results using 200 grid points are shown in Figure 1 (for the sake of better resolution only $r \in [0, 0.15]$ is plotted). As has also been found by SN, an anomalous spike occurs in the density in the first few zones near the origin (see the dotted-dashed line). Recently, Mönchmeyer and Müller (1989) demonstrated that the error at the origin is a result of using a coordinate-centred staggered mesh. They found that, although the analytic solution yields the radial momentum density ρv_r as a linear function of the radius r , the finite-difference representation $\langle \rho v_r \rangle_i$ becomes an increasingly non-linear function of r towards the origin $r = 0$ (cf. equations (2.41), (2.42) of Mönchmeyer and Müller, 1989). Therefore, momentum and matter are advected towards the centre with increasing velocities which results in the anomalous density spike.

However, if the last term in equation (2.41) of Mönchmeyer and Müller (1989) is multiplied by the correction factor

$$f^{\text{corr}} = r_i \left(\frac{3 \tilde{r}_i^4 - \tilde{r}_{i-1}^4}{4 \tilde{r}_i^3 - \tilde{r}_{i-1}^3} \right)^{-1}, \quad (14)$$

the radial momentum density becomes a linear function of radius r . Thus, using ZEUS-2D notation and noticing that the radial momentum density corresponds to the specific momentum $s_1 = \rho v_1$ in ZEUS-2D, one finds that the left-hand side of equation (62) of SN should be multiplied by the correction factor

$$f_i^{\text{corr}} = g2a_i \left(\frac{3 g2b_i^4 - g2b_{i-1}^4}{4 g2b_i^3 - g2b_{i-1}^3} \right)^{-1}. \quad (15)$$

Note that in cylindrical and Cartesian geometries f_i^{corr} must be set to unity.

The result of the pressure-free collapse of a sphere as computed by ZEUS-2D with the correction factor f_i^{corr} is shown by the dashed line in Figure 1 (using the same spatial and time steps as before). The anomalous spike near the origin totally disappears, which proves the necessity of specific momentum corrections in ZEUS-2D. This technique was first found to be successful in suppressing the anomalous density spike by Boss and Myhill (1992).

The correction f_i^{corr} was derived for the specific case of the pressure-free collapse of a sphere with the radial velocity being linearly dependent on the radius. In the case of isothermal or non-isothermal collapse of interstellar clouds the radial velocity was found to be almost linear near the origin. Thus, the use of the correction factor f_i^{corr} may be expected to reduce drastically the magnitude of the anomalous spike.

2.2.3 Moving Mesh

In many cloud collapse applications the computational mesh has to be moved with the fluid to maintain better resolution near the origin. Thus, if we allow the mesh to collapse with the cloud by setting the grid velocity vectors equal to the fluid velocity at every gridpoint (except for the boundaries), then the net density flux through the control volume interfaces is equal to zero and advection errors disappear. Obviously, in this case there is no need to use the corrections described above.

Unfortunately, such a nice situation remains only in the spherically symmetric case. In two dimensions, however, the grid velocity vectors at each slice in Θ at a given r must be identical to preserve orthogonality. Thus, a common choice is (using ZEUS-2D notation of SN)

$$vg1_i = \frac{1}{j0 - j_i} \sum_{j=j_i}^{j0} v1_{i,j}. \quad (16)$$

It is clear now that the grid velocities in each grid slice in r do not necessarily coincide with the fluid velocity at each gridpoint, and the density flux through the control volume interfaces is non-zero.

In fact, this may lead to even higher numerical errors in the density at the origin than in the case of a non-moving mesh. For example, if the grid velocity is equal to half of the fluid velocity at each corresponding gridpoint (Figure 2, dashed line), then the anomalous density spike at the origin is even higher than in the case of a non-moving mesh (Figure 1, the dotted-dashed line). Indeed, any mesh motion will

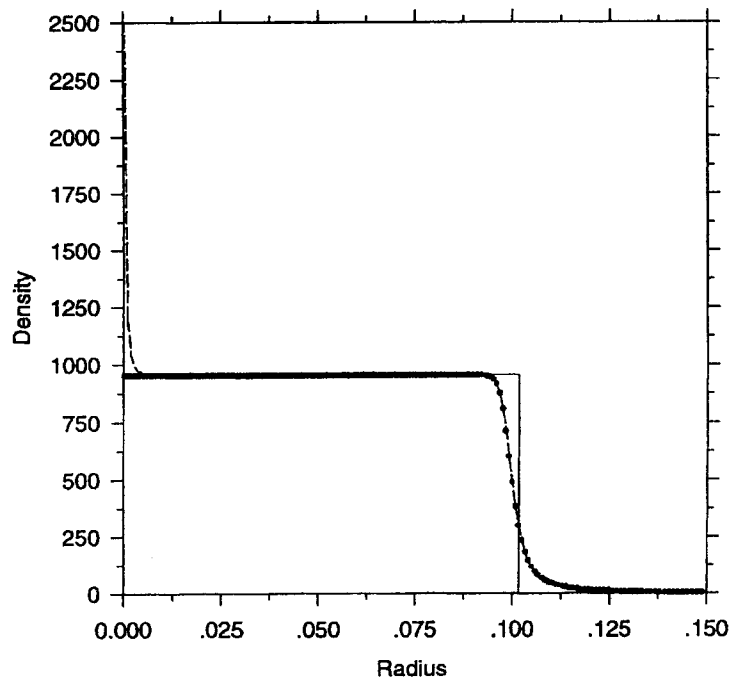


Figure 2 The density distribution for the pressure-free collapse of a homogeneous sphere at $t = 0.985$ free-fall times using a moving mesh. The grid velocity is equal to half of the fluid velocity at each corresponding gridpoint. If the momentum density correction is not used, an anomalous density spike develops near the origin (dashed line). With the inclusion of the momentum density correction, the numerical solution becomes indistinguishable from the analytical one except for the region near the outer moving boundary (filled circles). The analytic solution is denoted by the solid line.

result in the grid compression near the origin, and thus in the zone size decrease as compared to the case of a non-moving mesh. The latter will immediately result in the increase of the spurious matter and momentum transfer, as it directly follows from equations (2.42) and (2.43) of Mönchmeyer and Müller (1989). However, if the momentum density correction is used the anomalous spike vanishes and the numerical solution is indistinguishable from the analytic one except for the region near the outer moving boundary (Figure 2, filled circles).

2.2.4 Sod Shock-Tube Test

The second one-dimensional test is a Sod shock-tube problem, which tests all the transport and source terms including artificial viscosity. To compare with the results of SN we set up two discontinuous states, a hot dense gas on the left and a cool rarefied gas on the right, at $t = 0$, and let them interact. The initial conditions and the number of zones in a computational area are the same as in the paper of SN.

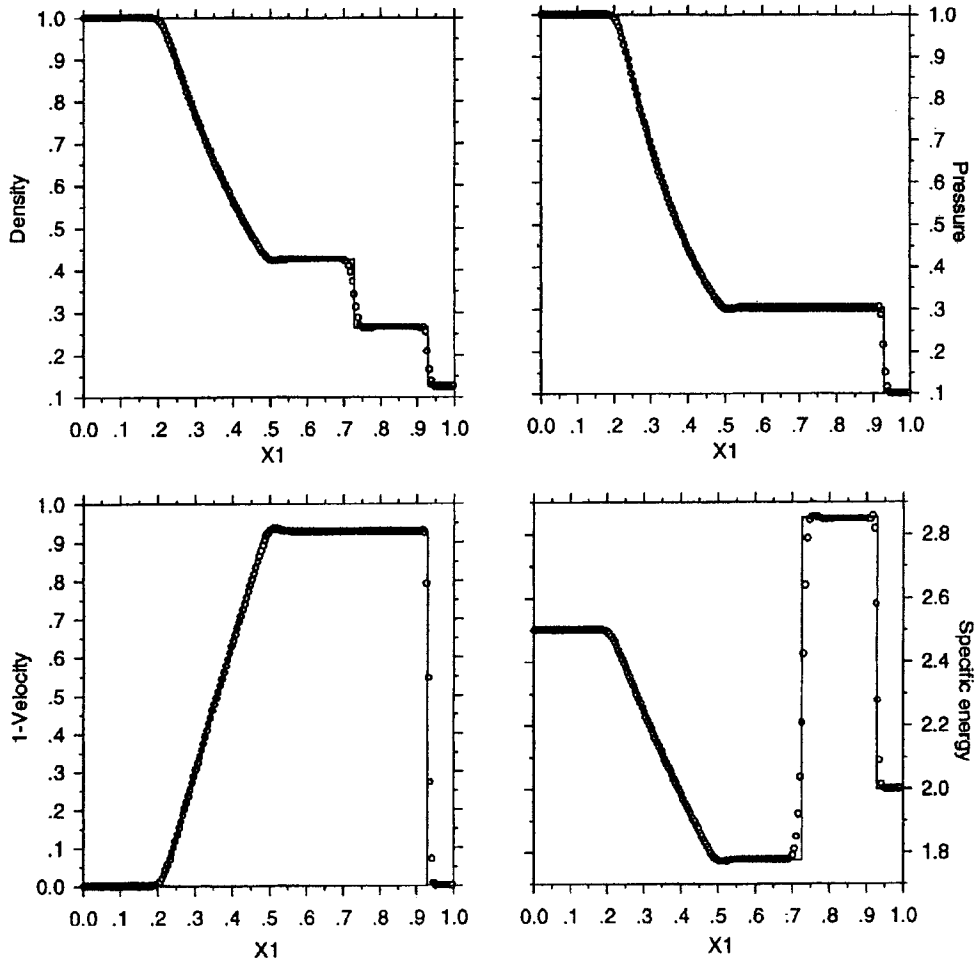


Figure 3 Results for the density (*top left*), pressure (*top right*), velocity (*bottom left*), and specific internal energy e/ρ (*bottom right*) for the Sod shock-tube problem at time $t = 0.245$. In each case, the analytic solution is plotted as a solid line.

As a test of a numerical algorithm, the shock-tube problem demonstrates whether the code can give the correct jump conditions and whether the artificial viscosity is capable of damping the oscillations that occur after the shock front, and at the same time not smearing the shock to an unacceptable degree. The results of the test are shown in Figure 3, where the solid line denotes the analytic solution to the shock-tube problem given by Hawley, Smarr, and Wilson (1984). Our results agree well with the test results obtained by SN (1992), having inherited the same numerical errors (e.g. overshoots). Also, it can be noticed that the amplitude of the specific energy fits better to the analytic solution than in the similar test of SN.

3 COLLAPSE OF NON-ISOTHERMAL, NON-ADIABATIC INTERSTELLAR CLOUDS

3.1 *Initial and Boundary Conditions*

Interstellar gas, unlike stars and other compact objects, has a low density and occupies a large volume, so that the energy released in the form of photons travels far from its place of origin, usually leaving the object where it originated. Thus, a cloud loses its internal energy throughout its entire volume and the speed of this process is characterized by the cooling rate Λ (ergs cm⁻³ s⁻¹). The opposite process which takes place in the interstellar gas is volume heating due to background electromagnetic radiation and cosmic rays. It is characterized by the heating rate Γ (ergs cm⁻³ s⁻¹). In general, $\Gamma \neq \Lambda$ due to dynamical motions in the ISM and, therefore, the interstellar clouds are non-adiabatic objects by nature. However, at the initial stage of collapse the cooling and heating characteristic times are much smaller than the dynamical time and the initial temperature distribution can be obtained by assuming a cloud to be initially in thermal equilibrium with $\Gamma = \Lambda$. In general, the cloud is initially non-isothermal.

In the ZEUS-2D code, the boundary conditions are set by specifying the values of dependent variables in the ghost zones to be used by higher-order interpolation methods in the transport step (SN). The exact form of the boundary conditions applied depends upon the geometry and physics of the problem being solved. For a spherically symmetric geometry the inner boundary condition is essentially a reflecting one, thus the mass density and internal energy density in the ghost zones are set equal to the corresponding values of their images among the active zones, while the velocity is set to zero on the boundary and reflected for the second ghost zone. The outer boundary conditions, on the other hand, are determined by physics of the problem. The common approach (Larson, 1969) is to assume that a cloud has a fixed outer boundary, thus allotting a constant volume (and total mass) to it (the so-called constant volume boundary condition). This leads to $v_r = 0$ at the outer boundary of the computational domain. This approach is strictly valid only for an isolated cloud in empty space. It is to be expected that such conditions may develop in some cases of star formation (Woodward, 1978).

Another approach is to assume that a cloud is embedded in a diffuse interstellar medium of number density ~ 0.1 cm⁻³ and temperature $\sim 10^4$ K which provides a constant outer pressure of order 10^{-13} dyn cm⁻². This constant outer pressure boundary condition is most commonly used in Lagrangian hydrodynamics codes. However, in Eulerian codes it is rather difficult to implement this condition properly because the computational boundaries remain fixed in space. To study the effect of outer constant pressure on the dynamics of collapsing clouds with Eulerian codes in full generality, one should use the approach of Winkler and Norman (1986) who included the outer diffuse matter into the computational domain and treated the interstellar dense cloud and diffuse medium as two different phases using the technique of fractional volumes.

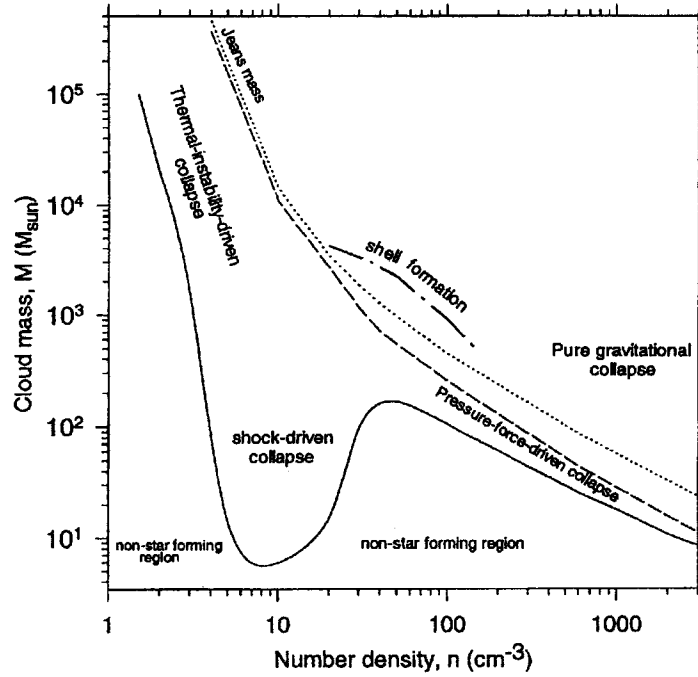


Figure 4 Initial number density – mass ($n_0 - M$) diagram for non-isothermal interstellar clouds. The solid line shows the minimum mass M_{\min} of a cloud unstable to collapse as a function of the initial number density n_0 . The dashed line (dotted line) is the Jeans mass of a cloud of initial number density n_0 , mass M , and inner temperature T^{in} (outer temperature T^{out}). The dotted-dashed line shows the minimum mass of a cloud intrinsically unstable to shell formation.

In this paper we have used the constant volume outer boundary condition in order to identify the physical effects inherent to the cloud itself and avoid the complicated influence of the outer diffuse matter on the cloud dynamics.

3.2 The Effect of Temperature Gradients – Lowering of the Jeans Mass

The critical mass of an isothermal cloud unstable with respect to gravitational collapse is determined by the well-known Jeans criterion; i.e., $\tau_{\text{ff}} < R/v_{\text{sound}}$, where $\tau_{\text{ff}} = (3\pi/32G\rho_0)^{1/2}$ is the free-fall time (Hunter, 1962), R is the radius of the cloud, and v_{sound} is the speed of sound. The Jeans mass is then

$$M_{\text{Jeans}} = \left(\frac{\gamma RT \pi^2}{8G} \right)^{3/2} \left(\frac{3}{4\pi\rho} \right)^{1/2}, \quad (17)$$

where R is the universal gas constant, G is the gravitational constant, T is the temperature, and γ is taken to be 5/3. As has been pointed out above, the interstellar cloud is usually non-isothermal. Therefore, it would be interesting to see

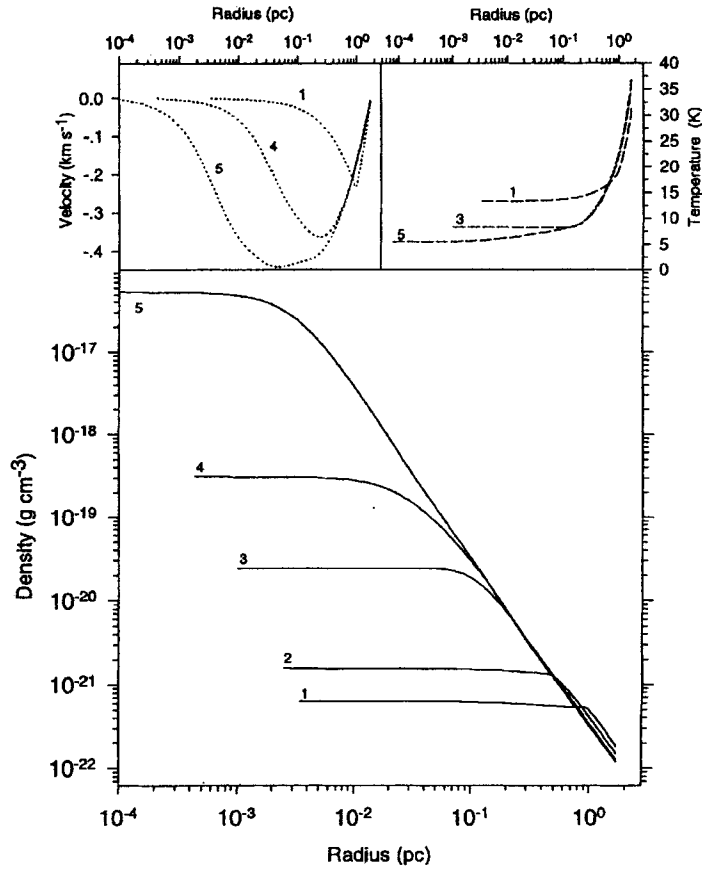


Figure 5 Collapse of the interstellar cloud of initial number density $n_0 = 200 \text{ cm}^{-3}$ and mass $M = 100 M_\odot$ shown at five different times: 1 ~ 1.43 Myr, 2 ~ 2.15 Myr, 3 ~ 2.8 Myr, 4 ~ 3.03 Myr, and 5 ~ 3.14 Myr. The density distribution is almost homogeneous in the collapsing core and drops down as $1/r^2$ in the envelope.

what effect a non-uniform temperature distribution and resulting pressure gradients have on the dynamical behaviour of interstellar clouds of different masses and densities.

The solid line in Figure 4 shows the variation of the minimum mass of a non-isothermal cloud, which can collapse under its own gravity, as a function of the initial number density, whereas the dashed line (dotted line) is the Jeans mass as a function of the initial cloud density ρ_0 and initial inner temperature T_0^{in} (initial outer temperature T_0^{out}). The lowering of the Jeans mass due to the temperature gradients, first pointed out by Tarafdar *et al.* (1985, 1989), is clearly visible. However, in contrast to their calculations, which used a Lagrangian code, the present results show that the lowering of the Jeans mass is highly non-monotonic. The difference may be due to inadequate treatment of shocks in their Lagrangian code.

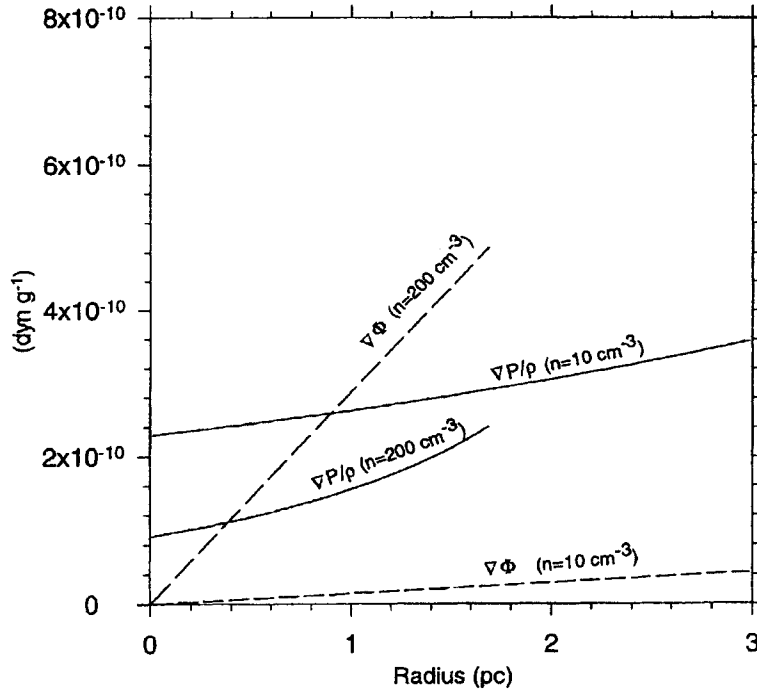


Figure 6 The initial pressure gradient force per unit mass $\nabla p/\rho$ (the solid line) and initial gravity force per unit mass $\nabla\phi$ (the dashed line) plotted for two clouds of $M = 28M_{\odot}$, $n_0 = 10 \text{ cm}^{-3}$ and $M = 100M_{\odot}$, $n_0 = 200 \text{ cm}^{-3}$, respectively.

Figure 4 shows that there are three distinct regions of initial cloud densities for which the non-isothermal temperature distribution plays an important role and gives rise to different phenomena.

3.2.1 Collapse due to Pressure Gradients

First, let us consider the collapse of homogeneous, non-isothermal clouds of initial densities $50 < n_0 < 3000 \text{ cm}^{-3}$ and masses lying between the Jeans curve (dotted line) and solid line (Figure 4). This region will be referred to as the pressure-force-driven collapse for the reason given below. Figure 5 shows the density, temperature, and velocity distribution of the collapsing interstellar cloud of $M = 100M_{\odot}$ and $n = 200 \text{ cm}^{-3}$ at different times. The density distribution exhibits the classical behaviour with the homogeneous central core and the envelope whose density is proportional to $1/r^2$. If this cloud were isothermal with the initial temperature equal to the lowest value $T = 16 \text{ K}$ (at the centre), it would have the Jeans mass equal to $111M_{\odot}$ (Figure 4, dashed line) and could not collapse to form a protostar. Note that we give here the lowest estimate for the Jeans mass, with the highest being equal to $216M_{\odot}$ for the outer cloud's temperature of 25 K (Figure 4, dotted

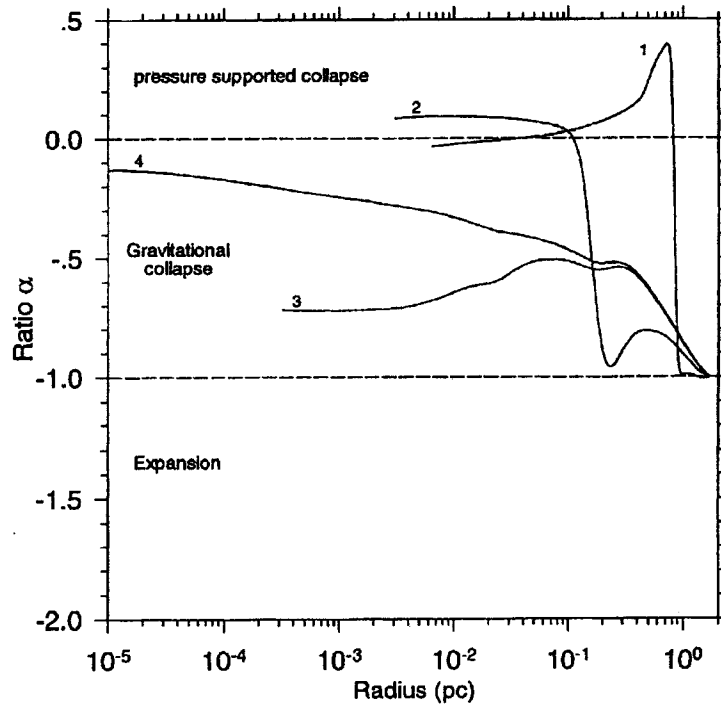


Figure 7 The ratio $\alpha = \nabla p / \rho \nabla \Phi$ of the pressure force per unit mass to the gravity force per unit mass as a function of radius for the gravitational collapse of the interstellar cloud of $M = 100M_{\odot}$ and $n_0 = 200 \text{ cm}^{-3}$ shown at four different times: 1 ~ 1.6 Myr, 2 ~ 2.7 Myr, 3 ~ 3.1 Myr, and 4 ~ 3.18 Myr.

line). The reason why it ultimately collapses can be understood from the following considerations. For our sample cloud of $M = 100M_{\odot}$, $n = 200 \text{ cm}^{-3}$ and $R = 1.7$ pc the initial temperature T_0 spans the range from 16 K in the centre to 25 K at the outer boundary. This initial temperature gradient gives rise to the inward (positive) pressure gradient force per unit mass $\nabla p / \rho$ (Figure 6, solid line), which in turn gives the matter an additional inward radial momentum. As can be seen in Figure 7 (plots 1, 2), this additional inward force promotes gravitational collapse at the first stages of dynamical evolution leading to a higher degree of cloud compression than in the case of isothermal collapse, so that the initially Jeans stable cloud becomes unstable and collapses to form a protostar. After about 2.8×10^7 yr the inward pressure gradient force disappears yielding the way to the outward pressure gradient force (as in the case of an isothermal cloud collapse), which is however too small to prevent the cloud from further gravitational contraction (Figure 7, plots 3, 4).

The dynamical evolution of the cloud of initial number density $n = 200 \text{ cm}^{-3}$ and mass $M = 55M_{\odot}$ which is lower than the critical mass in Figure 4 (the solid line), is plotted in Figure 8. The initial contraction (with the core density increase of about two orders of magnitude) is ultimately followed by the expansion phase to the almost

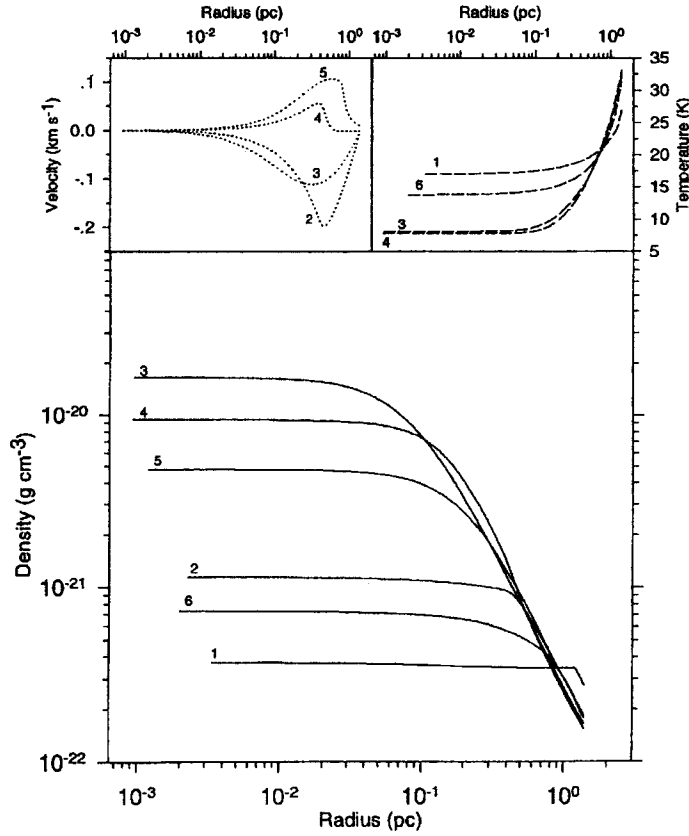


Figure 8 Non-star-forming evolution of the cloud of mass $M = 55M_{\odot}$ and number density $n_0 = 200 \text{ cm}^{-3}$ plotted at six successive times: 1 ~ 0.4 Myr, 2 ~ 1.9 Myr, 3 ~ 2.6 Myr, 4 ~ 2.9 Myr, 5 ~ 3.3 Myr, and 6 ~ 4 Myr. Initial contraction is followed by the expansion phase. The latter manifests itself as a positive velocity distribution.

initial diffuse state. As can be seen from Figure 9, which plots the ratio of pressure force to gravity force $\alpha = \nabla p / \rho \nabla \Phi$, the initial contraction is due to the inward pressure force acting at the first stages of dynamical evolution (Figure 9, plots 1, 2, 3). At the same time the inner most layers of the cloud become gravitationally unbound, because the outward pressure force overcomes the inward gravitational force $\alpha < -1$, and this tendency exists until all the cloud becomes gravitationally unbound and starts to expand (Figure 9, plot 4, 5). Further dynamical evolution is rather uncertain and probably depends on the initial conditions as well as on the mass and density of the cloud. At least clouds with masses slightly smaller than the critical mass given by the solid line in Figure 4 can exhibit clear oscillatory behaviour with successive contractions and expansions. When the cloud reaches its maximum contraction phase, the core density can be 10^2 – 10^3 times higher than the density at its maximum expansion phase (Prasad *et al.*, 1991).

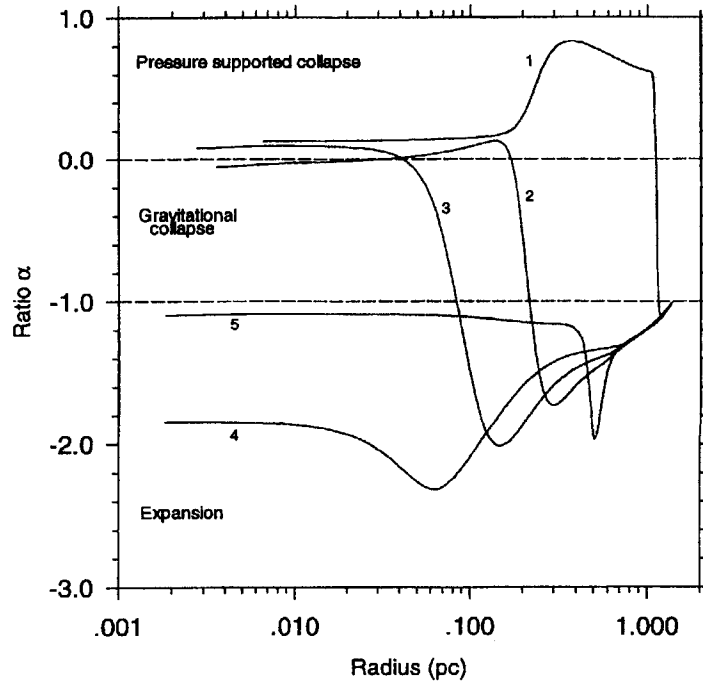


Figure 9 The ratio $\alpha = \nabla p / \rho \nabla \Phi$ of the pressure force per unit mass to the gravity force per unit mass as a function of radius during the dynamical evolution of the interstellar cloud of $M = 55M_{\odot}$ and $n_0 = 200 \text{ cm}^{-3}$ shown at five different times: 1 ~ 0.6 Myr, 2 ~ 2.2 Myr, 3 ~ 2.5 Myr, 4 ~ 2.8 Myr, and 5 ~ 4.1 Myr.

While the reversal of collapse is readily understandable and seems likely in real clouds, the successive oscillations are much less likely, because real clouds may not be conservative systems and various dissipative mechanisms can be present which may ultimately suppress the oscillations. Following Prasad *et al.* (1991) we shall refer to the area below the critical mass in Figure 4 as the non-star-forming region.

3.2.2 Shock-driven Collapse

As can be seen from Figure 4, the lowering of the Jeans mass is non-monotonic and most effective for interstellar clouds of low densities $5 < n_0 < 50 \text{ cm}^{-3}$. Figure 10 shows the density, temperature, and velocity (the ratio of the radial velocity v_r to the speed of sound v_s) distribution for the sample interstellar cloud of $M = 28M_{\odot}$ and $n = 10 \text{ cm}^{-3}$ during its dynamical evolution. At the first stages of evolution a compression wave develops, which then propagates inward and steepens to become a shock wave (shown by the arrow in Figure 10). The shock front appears in this figure as a discontinuity in the density and velocity distribution smeared over 2–3 computational zones due to an artificial viscosity. This low intensity Mach ~ 1.5 shock wave compresses and sweeps up the matter to the core, which after a

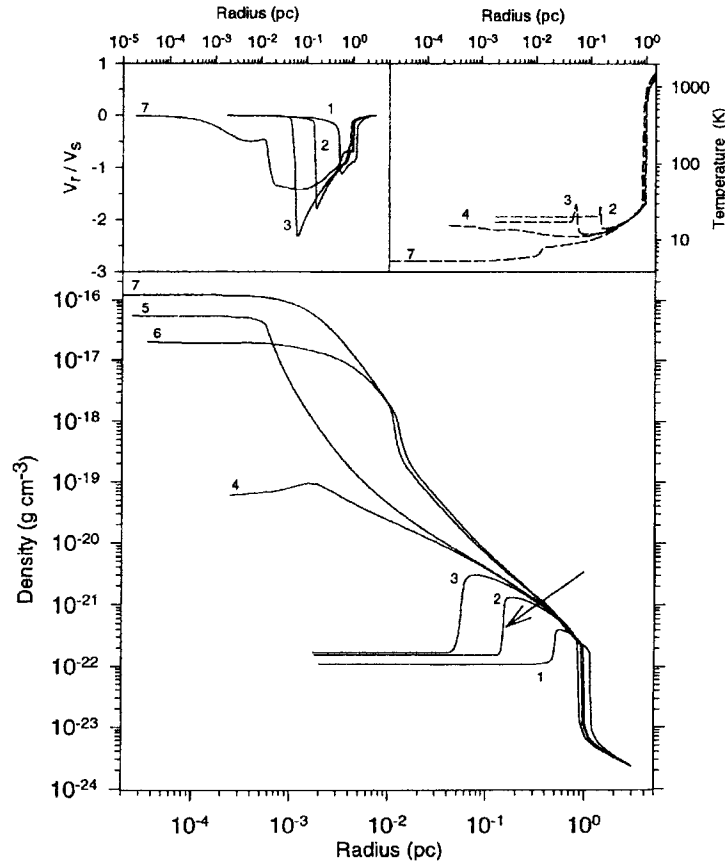


Figure 10 Shock-driven collapse of the interstellar cloud of number density $n_0 = 10 \text{ cm}^{-3}$ and mass $M = 28M_\odot$ plotted at seven successive times: 1 ~ 4.5 Myr, 2 ~ 4.9 Myr, 3 ~ 5 Myr, 4 ~ 5.05 Myr, 5 ~ 5.1 Myr, and 7 ~ 5.2 Myr. A well-developed shock wave c^* Mach ~ 1.8 is shown by the arrow.

small period of rebound becomes gravitationally unstable and collapses to form a protostar.

In Figure 11 we plot the ratio of the pressure force per unit mass to the gravity force per unit mass $\alpha = \nabla p / \rho \nabla \Phi$ as a function of radius for the same sample interstellar cloud. The insert in Figure 11 shows a very large value of $\alpha \sim 1000$ –2000 which monitors the presence of the shock wave propagating to the centre. However, at the same time the core is not gravitationally bound $\alpha < -1$ (in full agreement with the Jeans criterion for the cloud of $M = 28M_\odot$ and $n = 10 \text{ cm}^{-3}$) and tends to expand outward (Figure 11; plots 1, 2). After the time $t \sim 5 \times 10^6$ yr the shock wave reaches the centre compressing the matter by about 5 orders of magnitude, thus triggering a pure gravitational collapse of the core $0 < \alpha < -1$ (Figure 11; plot 4). The ratio $\alpha < -1$ for the outer part of the cloud indicates

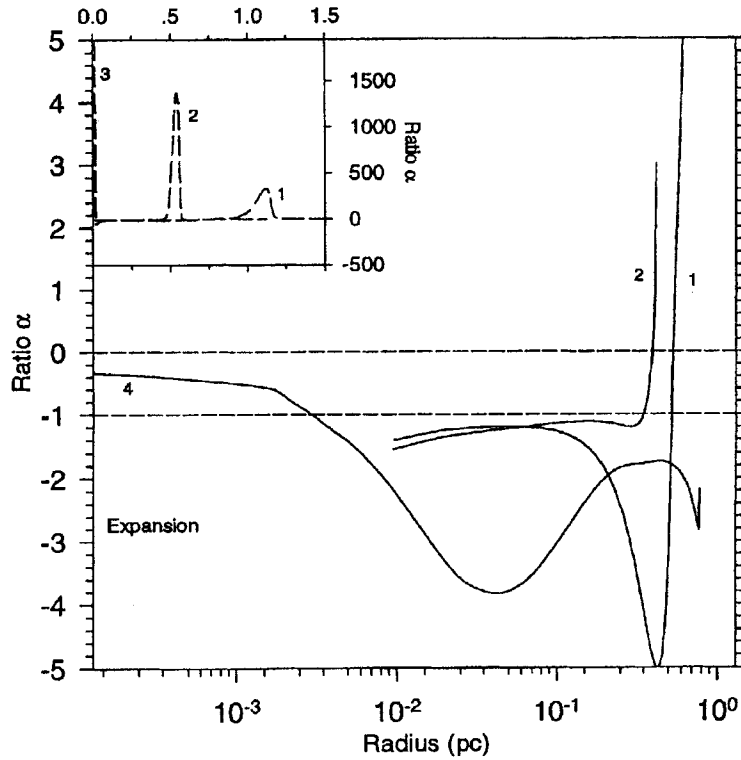


Figure 11 The ratio $\alpha = \nabla p / \rho \nabla \Phi$ of the pressure force per unit mass to the gravity force per unit mass as a function of radius for a shock-driven collapse of the interstellar cloud of $M = 28M_{\odot}$ and $n_0 = 10 \text{ cm}^{-3}$ shown at four times: 1 ~ 3.9 Myr, 2 ~ 4.9 Myr, 3 ~ 5.1 Myr, and 4 ~ 5.22 Myr.

that it is not gravitationally bound (plot 4; Figure 11). However as the shock wave passes through the cloud, it gives the matter a high inward momentum. Thus, the outer part still falls onto the core, though with gradual deceleration. The mass of the collapsing core is about $0.4M_{\odot}$ which corresponds to $\sim 1.5\%$ of the initial cloud mass.

To understand the reason why a shock wave occurs during the dynamical evolution of interstellar clouds of densities $5 < n_0 < 50 \text{ cm}^{-3}$, let us again look at Figure 6. In the case of a low-density cloud $n = 10 \text{ cm}^{-3}$ the initial inward pressure force per unit mass $\nabla p / \rho$ is larger than in the case of a high-density cloud $n = 200 \text{ cm}^{-3}$, whereas the gravity force per unit mass $\nabla \Phi$ is relatively small. Therefore, the former plays a dominant role, and because at the first stage of dynamical evolution the pressure gradient ∇p is a non-linear, outwardly increasing function of radius, it gives rise to a pressure wave, which propagates inward and steepens to become a shock wave. This effect is similar to that found by Winkler and Newmann (1980) in their calculations of solar-type star formation and referred to as the formation of the first shock wave.

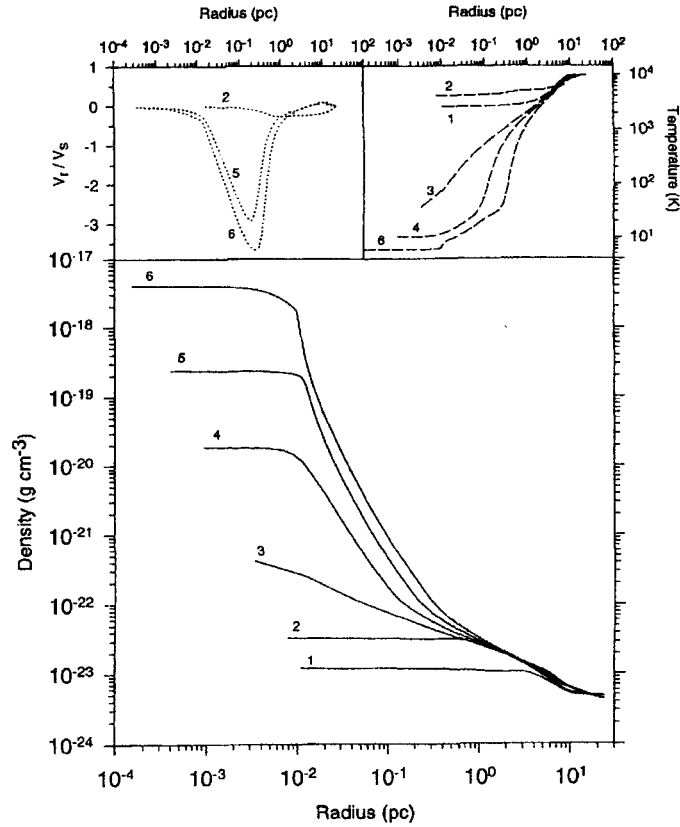


Figure 12 Thermal-instability-driven collapse of the interstellar cloud of mass $M = 4000M_{\odot}$ and number density $n_0 = 3 \text{ cm}^{-3}$ shown at six successive times: 1 ~ 0.7 Myr, 2 ~ 0.9 Myr, 3 ~ 1.5 Myr, 4 ~ 1.58 Myr, 5 ~ 1.71 Myr, and 6 ~ 1.83 Myr.

Although the non-linear pressure force $\nabla p/\rho$ also initiates a pressure wave in the case of an interstellar cloud of $n = 200 \text{ cm}^{-3}$, this pressure wave does not develop into a shock wave. The latter happens due to the fact that for the cloud of $n = 200 \text{ cm}^{-3}$ the gravity force plays a dominant role giving rise to the density and pressure increase at the core as in the case of isothermal collapse. The growing pressure at the core destroys the inequality $p_1 < p_2$, where p_1 and p_2 represent the pressure upshock and downshock, respectively – an essential condition for the shock wave to propagate.

This shock-driven collapse is to be distinguished from the compression of interstellar clouds by shock waves formed around H II regions. In the last case, the shock wave comes from outside, whereas in the first case it develops during the actual collapse due to non-linear inward pressure gradients, which in turn arise as the result of the finite transparency of interstellar clouds, and the heating effect of the background electromagnetic radiation always present in the ISM.

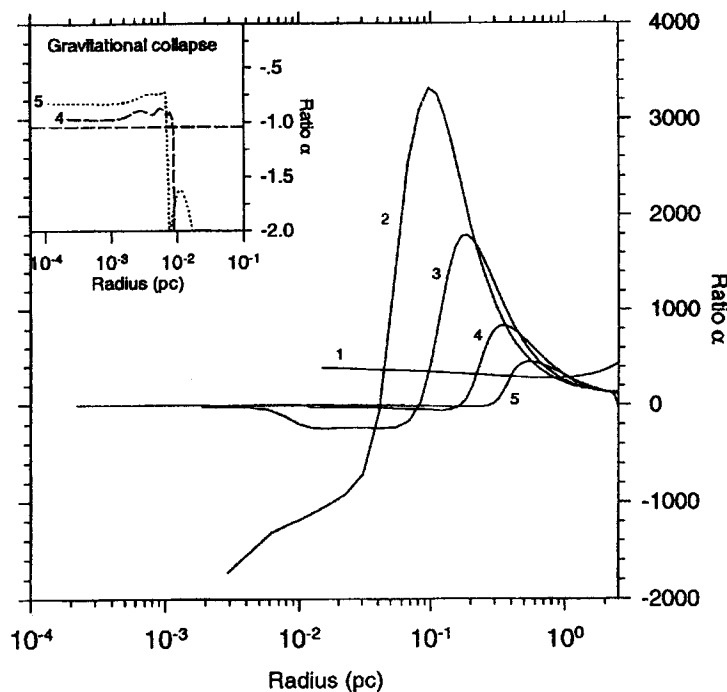


Figure 13 The ratio $\alpha = \nabla p / \rho \nabla \Phi$ of the pressure force per unit mass to the gravity force per unit mass as a function of radius during the dynamical evolution of the interstellar cloud of $M = 4000M_{\odot}$ and $n_0 = 3 \text{ cm}^{-3}$ plotted at five different times: 1 ~ 0.8 Myr, 2 ~ 1.53 Myr, 3 ~ 1.6 Myr, 4 ~ 1.83 Myr, and 5 ~ 1.86 Myr.

3.2.3 Thermal Instability and Collapse of Low-density Interstellar Clouds

As can be seen from Figure 4, the critical mass for the interstellar clouds of low densities $n \leq 5 \text{ cm}^{-3}$ sharply increases. This is due to the fact that the clouds of such low densities and masses of a few hundred solar masses or less become transparent to the outer electromagnetic radiation and heated to almost uniform temperature. Therefore, the pressure gradient force is small and cannot give rise to a shock wave and provide the core with the necessary degree of compression. Nevertheless, the critical mass shown by the solid line in Figure 4 is well below the Jeans mass shown by the dashed line. This indicates the presence of some other compression mechanism, which ultimately brings a gravitationally stable cloud to the point where it starts collapsing under its own gravity.

Figure 12 shows the density, temperature, and velocity (the ratio of the radial velocity v_r to the speed of sound v_s) distribution for the sample interstellar cloud of $M = 4000M_{\odot}$ and $n = 3 \text{ cm}^{-3}$ during its dynamical evolution. By the time $t \sim 1.6 \times 10^6$ yr, an almost homogeneous plateau develops near the centre with its density increasing very fast in time. Velocity profiles show the development of supersonic flow of Mach ~ 3 at later times near the centre of the cloud. All these

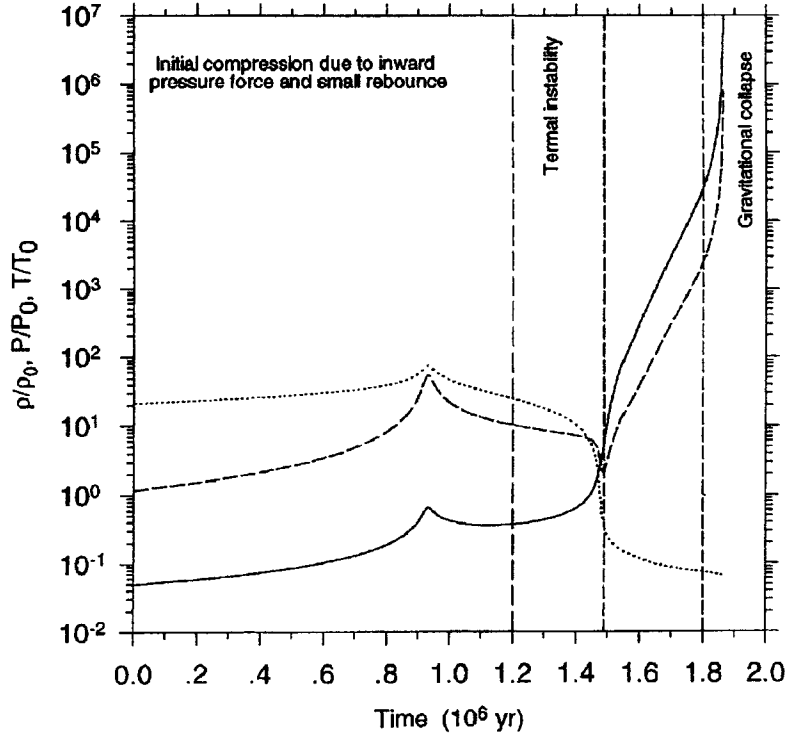


Figure 14 Time-dependent evolution of the density ρ (the solid line), pressure p (the dashed line), and temperature T (the dotted line) at the centre of the interstellar cloud of mass $M = 4000M_{\odot}$ and initial number density $n_0 = 3 \text{ cm}^{-3}$. The scaling factors are $\rho_0 = 10^{-22} \text{ g cm}^{-3}$, $p_0 = 6 \times 10^{-13} \text{ dyn cm}^{-2}$, and $T_0 = 80 \text{ K}$.

indicate the onset of gravitational collapse of the initially Jeans stable cloud. This collapsing core has the mass of $\sim 0.5M_{\odot}$ which is equivalent to $\sim 0.01\%$ of the initial cloud mass. Note that in this case there is no evidence of the development of a shock wave and the core is compressed to the critical density with the help of some other mechanism.

Figure 13 shows the dynamical evolution of the same interstellar cloud in terms of the ratio of the pressure gradient force per unit mass to the gravity force per unit mass $\alpha = \nabla p / \rho \nabla \Phi$. As can be seen from plot 1, the initial pressure force per unit mass $\nabla p / \rho$ is inward directed ($\alpha > 0$) and much larger than the gravity force per unit mass $\nabla \Phi$, so that $\nabla p / \rho$ acts to compress the matter in the centre of the cloud. For the time being, a very large inward pressure force develops near the centre $0.05 \leq r \leq 2 \text{ pc}$ (hereafter referred to as a pressure force spike), whereas in the centre the outward pressure force starts opposing the gravity ($\alpha < -1$). The inward pressure force pushes the matter towards the centre contributing to a density increase in the core. Thus, the ratio α gradually decreases approaching the critical value $\alpha = -1$, where gravitational collapse occurs. By the time $t \sim 1.8 \times 10^6 \text{ yr}$,

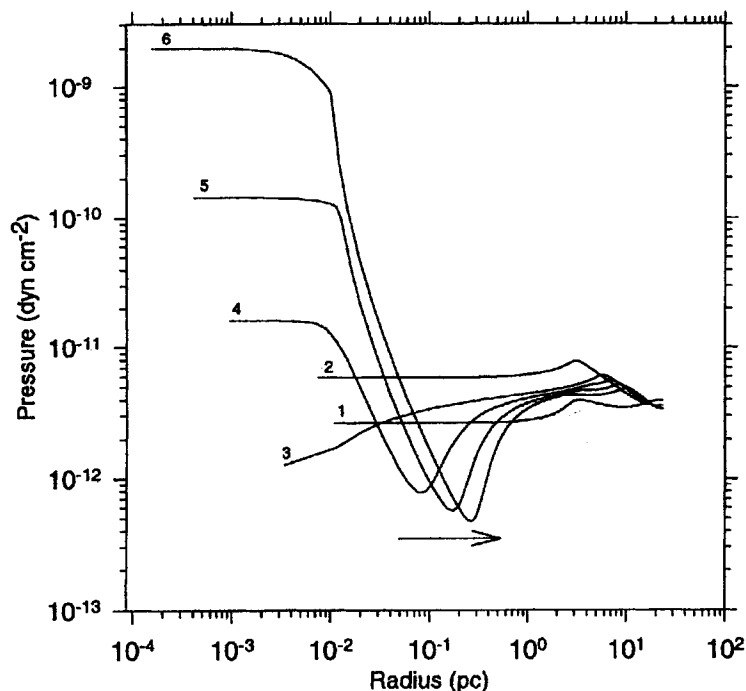


Figure 15 Pressure distribution during the collapse of the interstellar cloud of mass $M = 4000M_{\odot}$ and initial number density $n_0 = 3 \text{ cm}^{-3}$ plotted at the same times as in Figure 12. The arrow shows the direction of propagation of the density gap caused by thermal instability.

the density reaches its critical value and the core starts collapsing under its own gravity, which corresponds to $0 < \alpha < -1$ (Figure 13; insert, plots 4 and 5). Note that in contrast to the shock-driven collapse, where such a pressure force spike moves inward in accordance with the actual shock position and grows in magnitude as the shock intensity increases (Figure 11; insert), here the pressure force spike propagates outward, decreasing gradually in magnitude (Figure 13, plots 2, 3, 4, and 5).

To understand the reason why this large inward pressure force develops, let us look at Figure 14, which shows the time evolution of the density, pressure, and temperature at the centre of the interstellar cloud of $M = 4000M_{\odot}$ and $n = 3 \text{ cm}^{-3}$. During the time $t \leq 9 \times 10^5 \text{ yr}$ the density and pressure are growing due to the initial inward pressure force $\nabla p/\rho$, while the temperature remains almost constant. At the time $t \sim 9 \times 10^6 \text{ yr}$ the pressure force changes its sign at the centre of the cloud, becomes outward directed, and starts opposing the gravity. The latter results in a small rebound. However, after the time $t \sim 1.2 \times 10^6 \text{ yr}$ the density starts growing again, while the pressure is decreasing. The latter happens to be due to very effective cooling at number densities $n \sim 20\text{--}120 \text{ cm}^{-3}$, so that the temperature falls by about two orders of magnitude in a short period of time $\sim 10^5 \text{ yr}$ initiating

a sharp pressure decrease in the centre of the cloud. As a consequence, the inward pressure force develops (note, that the density in the layers slightly away from the centre has not yet reached the necessary value for effective cooling to occur). This inward pressure force pushes the matter towards the centre (Figure 13), thus initiating a further density increase. The latter in turn leads to more effective cooling and, therefore, a further temperature and pressure decrease in the centre of the cloud. This unstable situation continues until the central density grows by about two orders of magnitude, where the cooling becomes not so effective to support the pressure decrease ($t \sim 1.5 \times 10^6$ yr, Figure 14). Then, the central pressure starts growing again and the process stabilizes. However, by that time the layers of the cloud neighbouring the centre have reached the necessary degree of compression and the above mechanism repeats there.

The phenomenon described above is well known as a thermal instability (Field, 1965). Figure 15 shows the development of a pressure gap associated with the thermal instability, so that the outer matter slides down this gap contributing to the density increase in the core. This pressure gap has a tendency to propagate outward, as shown by the arrow in Figure 15. As we believe, a good analogy can be a chain reaction with the initial inward pressure force increasing the core density of a cloud to its critical value and thus triggering the onset of thermal instability, which then propagates from inside out leaving in its wake matter of higher density. This process continues until the core density reaches the critical value and starts collapsing under its own gravity (Figure 14, $t \geq 1.5 \times 10^6$ yr; Figure 12, plot 6).

As one goes down the vertical line of specified density $n = 3 \text{ cm}^{-3}$ in Figure 4, the radius of the corresponding interstellar cloud decreases. Consequently, the initial temperature distribution approaches the isothermal one, for which the inward pressure gradient force becomes negligible. Therefore, when one comes to the critical line in Figure 4, the inward pressure force becomes so small that it cannot provide the core of the corresponding cloud ($\sim 1500M_{\odot}$ and $n = 3 \text{ cm}^{-3}$) with the necessary degree of compression for the onset of thermal instability ($n \geq 20 \text{ cm}^{-3}$), and the cloud bounces back to the almost initial diffusive state.

3.3 *The Effect of Higher Outer Electromagnetic Radiation*

The effect of higher outer electromagnetic radiation (ten times more than the normal radiation field adopted in the previous calculations) on the critical mass of a cloud unstable to gravitational collapse is shown by the solid line in Figure 16. The curve has shifted to the right and slightly down, so that the thermal-instability-driven collapse can now be triggered in the more dense clouds of $n \leq 35 \text{ cm}^{-3}$ as compared to the case of normal background radiation. Shock-driven collapse also occurs in a different range of initial number densities $35 < n < 400 \text{ cm}^{-3}$. Indeed, as the outer radiation increases, interstellar clouds of low density $n < 35 \text{ cm}^{-3}$ and low mass $m \leq \text{a few} \times 10^2 M_{\odot}$ become heated to almost homogeneous temperature. Consequently, the radial pressure gradients become not steep enough to initiate the development of a shock wave. On the other hand, as the density increases, the interstellar cloud becomes more and more opaque to the outer radiation. Connected

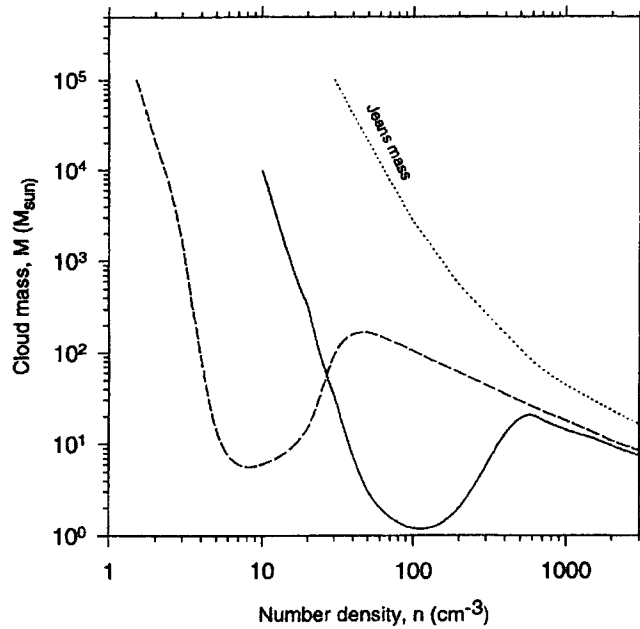


Figure 16 The minimum mass M_{\min} of a cloud unstable to collapse as a function of the initial number density n_0 . The dashed line corresponds to the background outer radiation field, whereas the solid line shows the effect of a higher outer radiation field (10 times the background one). The Jeans mass is denoted by the dotted line.

with the density increase, differentiation of the temperature between the central and outer part of the cloud leads to the development of steep radial pressure gradients, an essential condition for a shock wave to occur. Therefore, physical conditions for the development of a shock wave, namely the steep radial pressure gradients, are now met for more dense interstellar clouds of $35 < n < 400 \text{ cm}^{-3}$.

In the case of dense clouds $n > 500 \text{ cm}^{-3}$ a small lowering of the critical mass with respect to the critical mass for a normal radiation field (the dashed line) is also noticeable. This is probably associated with the steeper radial temperature distribution in the case of higher outer radiation field than in the case of a normal radiation field.

4 CONCLUSION

We have adopted the single-temperature approximation, because most of our calculations lie in the range of temperatures of 10–5000 K. In this range of temperatures the direct influence of ionization on hydrodynamics is small. However, ionization is important for cooling of the interstellar gas (cooling due to C II). We admit that strong shocks can ionize the interstellar gas and this process may be important

for an adequate treatment of interstellar chemistry. However, as can be seen in Figure 10, shocks in our calculations are weak, $\text{Mach} \approx 2$.

Magnetic fields are important for cloud collapse simulations. It is well recognized that magnetic fields play a crucial role in cloud dynamics and a diffuse cloud becomes gravitationally unstable by losing its magnetic support through ambipolar diffusion. But there is no clear evidence that sufficiently strong magnetic fields are present in every star-formation event. Thus, we decided to show some other mechanisms, purely hydrodynamical, that can push a diffuse, gravitationally stable cloud into a gravitationally unstable phase. To trace these purely hydrodynamical effects, we switch off magnetic fields.

In the present paper, for the sake of simplicity, we have adopted a constant volume outer boundary condition. An alternative choice, a constant outer pressure boundary condition, may influence the cloud dynamics if the time for a sound wave to propagate across the cloud is less than the cloud free-fall time (equation (11)). In this case the information from the outer boundary (sound waves) travels inward faster than the cloud can collapse (Bodenheimer and Sweigart, 1968). However, it is difficult to estimate the characteristic times in our case of non-isothermal collapse, because the temperature distribution is usually highly non-uniform. Preliminary computations show that the constant outer pressure boundary condition may influence the quantitative results and slightly change the shape of the solid line Figure 4. Nevertheless, the main qualitative results, i.e., such phenomena as pressure-force-driven collapse, shock-driven collapse, and thermal-instability-driven collapse, remain intact.

All three mechanisms that trigger the collapse of gravitationally stable clouds are initiated by the non-uniform temperature distribution. The degree of non-uniformity of the temperature distribution in turn depends on a variety of factors (cf. equations (5) and (6)) such as photoelectric heating efficiency of grains, grain charge, grain attenuation efficiency, cosmic ray heating rate, intensity of electromagnetic radiation, and depletion of such coolants as carbon, iron, and others. Thus, the interstellar grains play an important role in maintaining the non-uniform temperature distribution and hence in triggering the gravitational collapse of gravitationally stable interstellar clouds. This role of grains in cloud dynamics and star formation has not been recognized before.

The time evolution of the density and temperature distribution in the case of shock-driven and thermal-instability-driven collapse (Figures 10 and 12) is significantly different from that of pressure-force-driven collapse (Figure 5). Tarafdar *et al.* (1985) and Prasad *et al.* (1991) studied only the time evolution and spacial structure of molecular abundances for the case of pressure-force-driven collapse. The molecular abundances in the case of shock-driven and thermal-instability-driven collapse are expected to differ from those obtained by Tarafdar *et al.* (1985) and Prasad *et al.* (1991). It will be interesting to examine whether this difference can explain some of the peculiarities (sf. Ohishi, Irvine, and Kaifu, 1992) observed in interstellar clouds.

Therefore, the present study has revealed not only two new interesting mechanisms of protostar core formation due to thermal shock waves and thermal in-

stability, but also it has suggested a possible explanation of peculiar molecular abundances in the interstellar clouds.

Acknowledgements

Our special thanks go to Mike Bisset for reading the manuscript and suggesting valuable corrections. EIV thanks the Tata Institute of Fundamental Research for their hospitality. Thanks are also due to the Theoretical Astrophysics Group and especially to S. M. Chitre for providing good computational facilities. EIV would like to thank the International Centre for Fundamental Physics in Moscow for a support grant and the International Astronomical Union for a travel grant.

References

- Blitz, L. (1987) In: G. B. Morfill and M. Scholer (eds.), *Physical Processes in Interstellar Clouds*, Reidel, Dordrecht, p. 35.
- Bochkarev, N. G. (1992) *The Basics of Physics of Interstellar Matter*, Moscow, Izd. MGU, p. 146 (in Russian).
- Bodenheimer, P. (1968) *Astrophys. J.* **153**, 483.
- Bodenheimer, P. and Sweigart, A. (1968) *Astrophys. J.* **152**, 515.
- Boss, A. P. and Haber, J. G. (1982) *Astrophys. J.* **255**, 240.
- Boss, A. P. and Myhill, E. A. (1992) *Astrophys. J. Suppl. Ser.* **83**, 311.
- Boss, A. P. and Myhill, E. A. (1995) *Astrophys. J.* **451**, 218.
- Draine, B. T. (1978) *Astrophys. J. Suppl. Ser.* **36**, 595.
- Elmegreen, B. G. (1987) In: G. E. Morfill and M. Scholer (eds.), *Physical Processes in Interstellar Clouds*, Reidel, Dordrecht, p. 1.
- Field, G. B. (1965) *Astrophys. J.* **142**, 531.
- Harwit, M. (1988) In: M. Harwit, R. Kippenhahn, and J.-P. Zahn (eds.), *Astrophysical Concepts*, Springer, New York, p. 151.
- Hawley, J. F., Smarr, L. L., and Wilson, J. R. (1984) *Astrophys. J.* **277**, 296.
- Hunter, C. (1962) *Astrophys. J.* **136**, 594.
- Iben, I. Jr. (1965) *Astrophys. J.* **141**, 993.
- Larson, R. B. (1969) *Mon. Not. R. Astron. Soc.* **145**, 271.
- Mönchmeyer, R. and Müller, E. (1989) *Astron. Astrophys.* **217**, 351.
- Mouschovias, T. Ch. (1987) In: G. B. Morfill and M. Scholer (eds.), *Physical Processes in Interstellar Clouds*, Reidel, Dordrecht, p. 453.
- Norman, M. L. and Winkler, K.-H. (1986) In: K.-H. Winkler and M. L. Norman (eds.), *Astrophysical Radiation Hydrodynamics*, Reidel, Dordrecht, p. 187.
- Ohishi, M., Irvine, W., and Kaifu, N. (1992) In: P. D. Singh (ed.), *IAU Symposium 150 on Astrochemistry of Cosmic Phenomena*, Kluwer, Dordrecht, p. 171.
- Prasad, S. S., Heere, K. R., and Tarafdar, S. P. (1991) *Astrophys. J.* **373**, 123.
- Stone, J. M. and Norman, M. L. (1992) *Astrophys. J. Suppl. Ser.* **80**, 753 (SN).
- Tarafdar, S. P., Prasad, S. S., Huntress, W. T. Jr., Villere, K. R., and Black, D. C. (1985) *Astrophys. J.* **289**, 220.
- Tarafdar, S. P., Ghosh, S. K., Heere, K. R., and Prasad, S. S. (1989) *Highlights Astr.* **8**, 345.
- Tscharnuter, W.-M. and Winkler, K.-H. (1979) *Comput. Phys. Comm.* **18**, 171.
- van Leer, B. (1977) *J. Comput. Phys.* **23**, 276.
- von Neumann, J. and Richtmyer, R. D. (1950) *J. Appl. Phys.* **21**, 232.
- Winkler, K.-H. and Neumann, M. J. (1980) *Astrophys. J.* **238**, 311.
- Winkler, K.-H. and Norman, M. L. (1986) In: K.-H. Winkler and M. L. Norman (eds.), *Astrophysical Radiation Hydrodynamics*, Reidel, Dordrecht, p. 71.
- Woodward, P. R. (1978) *Ann. Rev. Astron. Astrophys.* **16**, 555.
- Woodward, P. R. and Colella, P. (1984) *J. Comput. Phys.* **54**, 115.